

ORIGINS OF PERSISTENT INTERACTION AMONG LOCALIZED CORROSION SITES

By Noah D. Budiansky and John R. Scully

Center for Electrochemical Sciences and Engineering
Department of Materials Sciences and Engineering
University of Virginia
Charlottesville, VA 22904

ABSTRACT

Interactions amongst localized corrosion sites were investigated using multi-electrode arrays. The 5x20 array consisted of one hundred 250 μm AISI 316 stainless steel wires configured into a close packed rectangle. Experiments were conducted in 0.05 M NaCl to investigate interactions triggered by the presence of active pits. Interactions between primary pits and the adjacent electrode surface were found to develop as regions of enhanced or suppressed pitting susceptibility originating from concentration and potential fields developed during growth of large pits, respectively. Aggressive species accumulation around active pits was also found to cause surface damage to electrodes that persisted for long periods of time after primary pits were repassivated. Oxide film alteration, inclusion damage, and surface contamination were all considered to be possible origins of persistent interactions. Persistent interactions were completely suppressed by nitric acid treatment. Sulfide inclusions were implicated to be the origin of such persistent interactions.

INTRODUCTION

It is often believed that pitting events are stochastic without any spatial or temporal effect on each other. However, as pits begin to form, the local environment changes [1]. Solution concentration and potential gradients develop that can affect pitting susceptibility on adjacent surfaces. These factors can also affect nearby oxide film and non-metallic inclusions to produce more permanent interactions. Taking into account these local changes, pitting can have a significant influence on the susceptibility of adjacent surfaces to localized corrosion. However, the time constant associated with each of these interactive processes differs [2-4].

Evidence of spatial interactions has been seen visually in the form of satellite pits that tend to form patterns around larger primary pits. Visual evidence of these pits can be seen on AISI 316 stainless steel that was anodically polarized in dilute chloride solution. As seen in Figure 1, a large pit has developed and formed circular zones indicating different degrees of pitting susceptibility on the nearby electrode surface. A region of suppressed pitting corrosion is observed in a concentric ring around a central large pit. Surrounding the suppressed region, a concentric ring of enhanced pitting corrosion is seen. These visual patterns indicate that interactions are occurring, but further investigations are required to determine their sources.

The use of multi-electrode arrays (MEA) have a significant advantage over planar electrodes due to the presence of separately addressable electrodes that enable spatial and

temporal information to be obtained simultaneously. Early studies using MEAs showed that experiments on closed-packed arrays of wires used to simulate a planar electrode could be conducted to study interactions between localized pitting events [2-4]. Studies may be conducted under potentiostat control or during galvanic coupling under open circuit conditions. Results from these studies indicated that as large primary pits grew stably on a given electrode or row of electrodes, a region of suppressed or enhanced pitting occurred on adjacent electrodes. These interactions depend on whether primary pits remained active or deactivated prior to localized corrosion susceptibility measurements. An increase in corrosion susceptibility, determined from a simple metric such as the pitting potential (E_{pit}) or the number of metastable pitting events, was seen adjacent to deactivated primary pits. In contrast, suppression was seen adjacent to primary pits that remained active. The limited number of electrodes and size of the MEAs, used during these studies, prevented determination of the full extent of spatially affected regions. Spatial modeling that incorporated these three interactions could produce patterns of damage on assumed homogenous electrodes [4].

At least three interactions have been hypothesized to occur due to phenomenon associated with localized pitting corrosion by the acid pitting mechanism [2-5]. As pits begin to form, anodic current flows from the pit as dissolution occurs. Metal ion hydrolysis takes place and H^+ ions are produced. In order to maintain electroneutrality, Cl^- ions are attracted to the pit area [1]. The consequences of pit stabilization are: (1) either cathodic polarization under open circuit conditions or ohmic potentials under potentiostatic or potentiodynamic polarization that suppress corrosion susceptibility adjacent to active pits, (2) increased pitting susceptibility caused by aggressive solution concentration, and (3) surface damage caused by exposure of the adjacent passive electrode to aggressive ions. Each of these interactions can operate on different length scales and different periods of persistency. These hypothesized origins are captured in a model of localized corrosion and explain the visual observations [2-4]. If these hypotheses are correct, then large active pits would be surrounded by a region of suppressed corrosion and further surrounded by a region of enhanced pitting. This hypothesis also suggests that interactions should have a persistent effect caused by nearly permanent surface damage where damage regions have a higher probability to pitting in the future. Significant persistent interactions were previously observed on 316 stainless steel [3]. However, the origin of such interactions was unknown.

EXPERIMENTAL

Interactive studies were conducted using AISI 316 stainless steel in the form of 250 μm wire fashioned into a multi-electrode array. The nominal composition of the wire was 0.13 % C, 0.31% Co, 18.18% Cr, 0.38% Cu, 1.75% Mn, 2.40% Mo, 12.25% Ni, 0.016% S, 0.35% Si, and the balance Fe. The wire contained non-metallic inclusions with a density of 0.00282 $\mu\text{m}^3/\mu\text{m}^3$ which a number density of between 20,000 and 200,000 inclusions/ cm^2 . These inclusions consisted of MnS and other mixed metal oxides and sulfides (Al_2O_3 , SiC, TiS, CrS, and FeS). Given the high Mn content of the stainless steel, it was assumed that the Cr content in the sulfides was less than 5% [6]. The inclusion area sizes ranged from less than 1 μm^2 to greater than 30 μm^2 with the majority of the inclusions between 1-3 μm^2 (Figure 2).

The as-drawn sample wire was coated with a cohesive polyamide coating that was 18 μm thick to prevent crevice corrosion and allowing wires to be placed in contact with each other while still ensuring electrical isolation. A close-spaced MEA was configured

in a 5x20 close packed simple cubic rectangle (Figure 3). The arrays were flush mounted in epoxy resin and polished with 600 grit polishing paper followed by a 1 μm alumina slurry polish. The samples were cleaned with ethanol in an ultrasonic bath to remove oils and any embedded alumina. Samples were placed in a face down horizontal configuration, in a custom designed electrochemical cell containing a remotely sensed saturated calomel reference electrode (SCE) and a platinum-niobium mesh counter electrode.

MEAs were tested in 0.05 M NaCl (3000 ppm) with a pH of 6.8 held at 47°C. A dilute 0.05 M NaCl was chosen to allow solution concentration enhancement to occur during interactive experiments. The test solution was held at 47°C to increase pitting susceptibility in the low halide concentration solution and to allow localized pitting corrosion to occur before transpassive corrosion or oxygen evolution. Solutions were made with reagent grade chemicals in 18 M Ω resistance water. The solutions were preheated in a water bath that also circulated heated water through a heating coil placed inside the custom built electrochemical cell.

Susceptibility to localized corrosion was determined using potentiodynamic scans to assess critical pitting potentials (E_{pit}). E_{pit} was taken as a convenient and accepted measure of resistance to pit stabilization. The electrodes in the MEAs were scanned from +0.1 V vs. OCP to +1.0 V_{SCE} at 1 mV/s to determine E_{pit} . E_{pit} was determined on each individual wire using a current threshold method since 100 samples were scanned during each MEA test. A current threshold of 10 μA was chosen because most electrodes showed a large current rise at this threshold, and few metastable pitting events reached this current [7, 8]. All E-I data determined to be above oxygen evolution or transpassive potentials was rejected and not included in any calculations. In order to treat the large data sets generated from MEA tests, cumulative probability analysis was used. Data populations that are normally distributed plot as straight lines on normal probability plots while skewed distributions show curved or bilinear lines suggesting different processes associated with pit stabilization. Analyzing the data at different points along the cumulative probability plots can be used to help elucidate information about the processes. Pitting potentials at cumulative probability of 25%, 50% (median), and 75% were analyzed for data populations. It can be speculated that a subset of the entire population of pits stabilized at low potentials are associated with highly susceptible inclusions while less susceptible inclusions or other sites stabilize at higher potentials. In order to increase population size and simplify results, data from either side of the active rows (Rows 11 and 12) were compiled together, i.e., rows 10 and 13 were compiled together and treated as identical. The data compiled in this way produced eight rows of resolution and E_{pit} associated with a given cumulative probability were plotted as distance from the active rows. Figure 3 shows a schematic of the close packed MEA indicating row numbers and the active rows.

Multi-Electrode Array Experiments

MEAs were tested in four different types of experiments. The first type of experiment was a non-interactive experiment where the entire MEA was scanned together to determine non-interactive control values to acquire baseline data for comparison. The OCP was measure for 15 minutes prior to determining the pitting potential. The other three types of experiments were designed to investigate interactions. Following measuring the open circuit potential, large pits were initiated on regions of the MEAs. The initiated regions were composed of two rows of five electrodes (ten working electrodes total) in the center of the MEA (rows 11 and 12), as seen in Figure 3. These

rows were held at +1.0 V_{SCE} for 15 minutes to initiate large stable pits that by pit coalescence approached the diameter of the wire electrodes. After the pits were initiated, three sets of tests were used to separate the hypothesized interaction effects: ohmic potential, aggressive species enhancement, and persistent surface damage [4]. The second type of experiment was designed to measure the effects of ohmic potential. Large pits were initiated on centrally located rows and potentiostatically held at +1.0 V_{SCE} to emit anodic currents greater than 100 μA . The remainder of the electrodes in the MEA, remaining in the passive state, were potentiodynamically scanned to determine E_{pit} . The third type of experiment was designed to explore the effect of aggressive species enhancement caused by the acid pitting mechanism. In order to separate aggressive species effects from ohmic potential effects, the centrally located pits were first held at +1.0 V_{SCE} for 15 minutes to initiate pits then deactivated and allowed to repassivate. Immediately after the initiated rows were deactivated, the remainder of the electrodes in the MEA were scanned to determine E_{pit} . The last set of experiments explored the persistent surface damage caused by prolonged exposure to aggressive species. After deactivating the initiated rows, the electrodes in the MEA were allowed to remain at the OCP. Rest periods of 15 minutes and 5 hours were used to allow prolonged exposure to the concentrated aggressive species. After the rest period and aggressive species dissipation, the remaining passive electrodes were potentiodynamically scanned to determine E_{pit} .

Surface modification

A series of experiments were conducted to investigate the effect of surface pretreatment on the subsequent pitting susceptibility. Electrodes were pretreated in acid solutions to modify the surface oxide and/or inclusions. MEAs were suspended face down separately in either 20% nitric acid and/or 1.0 M hydrochloric acid at room temperature for either five or 60 minutes prior to testing [9]. Nitric acid treatment was intended to remove MnS inclusions, which are a possible source of persistency [9]. Pretreatment with hydrochloric acid was used to mimic damage to passive electrodes adjacent to primary pits. After acid treatment, samples were rinsed briefly with distilled water and then placed in 0.1 M NaOH for 15 minutes to neutralize any residual acid solution and again rinsed with distilled water. After pretreatment, samples were immediately transferred to the electrochemical cell for testing.

RESULTS

In the first type of experiment, all 100 electrodes were scanned together to determine baseline E_{pit} data for non-interactive responses in solutions ranging from 0.05 to 5 M NaCl with pHs ranging from 1 to 7 at 47°C. The effect of pH and Cl^- concentration are shown in Figure 4. Data populations are tabulated as median E_{pit} and indicate that Cl^- concentration has a significant effect on E_{pit} values while pH has little effect above pH 5. A median E_{pit} value of +0.57 V_{SCE} in 0.05 M NaCl pH 6.8 at 47°C was used as the baseline value of E_{pit} . Deviation from this baseline was taken as evidence of interactions.

In order to determine the extent of interactions caused by the ohmic potential associated with current emitted from an active primary pit, a series of experiments were conducted with an active pit present. In order to simulate an active pit, two centrally located rows of the MEA were potentiostatically held to develop active pits. As active pits began to grow, current was generated from the pit causing a potential gradient to be

developed in solution along the surface of the electrode. The median values of the remotely sensed potential at which pits activated for each row of data were used to create Figure 5 to show the effects of ohmic potential as a function of distance from the active row. As seen in the Figure 5, a remotely measured critical potential, at a cumulative probability of 50%, increase of 250 mV was seen adjacent to the active row (row 1) with a gradual decrease with distance away from the active row. The increase was only 50 mV at the spatial limits of the MEA (Row 8). These results indicate that the ohmic potential field extends beyond eight rows from the active row. The ohmic potential effect is qualitatively similar at cumulative probabilities of 25%, 50%, and 75%. This suggests that the entire population of pits is effected equally by ohmic potential shielding. During the growth of the active pit, a concentration gradient of Cl^- and H^+ ions are also developed but is apparently overwhelmed by the ohmic potential field.

The concentration field plus the surface damage effects were separated from the ohmic potential effects by deactivating the active pits, in the third set of experiments. The measured potential in this case could be described as the ohmic potential (IR) free pitting potential since no ohmic potential gradient was present. As seen in Figures 6, E_{pit} of adjacent rows are compared to the non-interactive control. Results for rows 1 through 3 show a decrease in cumulative probability of pit stabilization at all potentials. This indicates that these rows are more susceptible. Cumulative probability for pit stabilization for rows 4 through 8 show little deviation from the non-interactive control. The E_{pit} data associated with three different cumulative probabilities, 25%, 50% (median), and 75% were examined. Median values indicate that a 300, 185, and 70 mV decreases in E_{pit} were seen for rows 1, 2, and 3 respectively. Rows 4 through 8 show E_{pit} values similar to the control case. E_{pit} vs. distance plots constructed from 25%, 50%, and 75% cumulative probability were qualitatively similar suggesting that the concentration field affects the entire population of pit sites.

In order to determine whether decreases in the remotely measured potential at which the current threshold was exceeded were caused by effects other than solution enhancement or surface modification (i.e., such as by cathodic polarization at nearby electrodes), a series of test were conducted that eliminated concentration gradients that were formed during pit row initiation. While two centrally located rows were initiated at +1.0 V_{SCE} for 15 minutes, the solution was stirred slowly. After 15 minutes, the active rows were deactivated, the solution stirring was stopped, and the remaining electrodes were scanned to determine the remote potential at which the current threshold was exceeded. Figure 8 shows that the E_{pit} for the slowly stirred results deviate by only ± 20 mV from the non-interactive control in 0.05 M NaCl. These results indicate that removal of the aggressive species gradient prevents increased susceptibility on adjacent regions as well as eliminate any long-term persistent memory effects. These results indicate that aggressive species play a critical role in promoting interactions among localized corrosion sites especially those that increase susceptibility.

The persistent effect of the concentration field was studied in the last set of experiments. Two rows of pits were initiated as in all other tests and then deactivated. Instead of immediately scanning the remaining electrodes, a rest period of 15 minutes or more at OCP was implemented to allow the aggressive species to alter the film or inclusions on adjacent electrodes and dissipate. After the rest period, the remaining electrodes were potentiodynamically scanned to determine E_{pit} . Figure 9 shows that the persistent interactive curve for 50% cumulative probability has an increase in pitting potential of 50 mV for row 1. Rows 2, 3, 4, and 5 show decreases in pitting potential of 30 mV, 50 mV, 100 mV, and 50 mV respectively compared to non-interactive control

values evaluated at 50% cumulative probability. Rows 6, 7, and 8 all show 20-40 mV increase above non-interactive control values. Evaluating cumulative probability curves indicate that the increase in E_{pit} on row 1 evaluated at 50% cumulative probability is not present when evaluating at 25%. Analysis at 25% indicates that decreases in E_{pit} of less than 20 mV is seen for row 1 while a decrease of 30 mV, 40 mV, 80 mV, and 40 mV are seen for rows 2, 3, 4, and 5, respectively, as shown in Figure 9. Rows 6, 7, and 8 all exhibit results similar to 50% cumulative probability. In contrast to Figures 6 and 7, where qualitatively the curves for 25%, 50%, and 75% are similar which suggests that the entire population of sites are affected, Figure 9 indicates that the populations of data at different distances are affected differently because curves are not qualitatively similar. These differences in interactions could be traced to differences in the critical defect associated with pit stabilization. It is speculated that interactions affect highly susceptible inclusions more severely than less susceptible inclusions. Hence, it is necessary to evaluate pit interactions at different cumulative probabilities.

The long-term persistence of surface damage was tested in the final set of experiments. Active pits were grown on two centrally located rows of the MEA for 15 minutes then deactivated. Following initiation the MEA was allowed to rest at the open circuit potential for five hours to allow all concentration gradients to dissipate. The experiment was design to test the long-term persistence of surface damage and to see if any repair occurs. In order to make a comprehensive comparison, MEAs were also subjected to non-interactive experiments where MEAs were subjected to five hours at open circuit potential prior to determining the potential at which the threshold current was exceeded. As seen in Figure 10, the non-interactive control value tested after five hours exposure at OCP increased to $+0.67 V_{\text{SCE}}$ compared to the standard non-interactive value of $+0.57 V_{\text{SCE}}$ after 15 minutes at OCP shown in Figure 7. The persistence experiment conducted after 5 hours shows a decrease in E_{pit} of 150 mV, 170 mV, and 110 mV for rows 1, 2, and 3, respectively. Rows 4 through 8 show less than 20 mV deviation from the non-interactive control conducted after five hours. Figure 10 indicates that there are still strong persistent interactions after five hours. Susceptibility adjacent to primary pits is still increased long after concentration fields were dissipated.

The origins of persistent interactions were investigated in a series of experiments that were designed to modify the surface of the electrodes in a controlled manner. In order to simulate the effect of acidity generated from metal ion hydrolysis during the growth of large pits according to the acid pitting mechanism, MEAs were pretreated with reducing HCl prior to testing. Other MEAs were pretreated in 20% HNO_3 to remove as many MnS inclusions as possible. MEAs were also pretreated in 1M HCl for 5 minutes and one hour to damage inclusions. Pretreatment with HNO_3 for one hour followed by HCl for one hour was also conducted to confirm that HNO_3 removed inclusions that would be susceptible to reducing HCl attack. After pretreatment the samples were treated with NaOH to neutralize any residual acid then rinsed with distilled water prior to testing. After pretreatment with HNO_3 or HCl, all the MEA electrodes were scanned to determine the remotely measured potential at which the current threshold was exceeded in 0.05 M NaCl. Figure 11 shows cumulative probability curves for the three experimental cases as well as the non-interactive control curve. As shown in Figure 11, the cumulative probability of pit stabilization at a given potential after HNO_3 pretreatment is slightly lower than the non-interactive control curve while the curves for HCl show increases in the cumulative probability at each potential. As expected, increasing the exposure time in HCl from five minutes to one hour further increases the cumulative probability of pit stabilization at each potential compared to non-interactive control curves.

The hypothesis that persistent interactions were caused by damage to MnS inclusions was investigated in the final series of experiments. MEAs were pretreated with HNO₃ for one hour to remove inclusions [9]. After pretreating, the MEAs were placed in 0.05 M NaCl and pits were initiated on two centrally located rows of electrodes. The MEAs were then exposed at the open circuit potential for 15 minutes to allow the concentrated species to damage inclusions and dissipate. After the concentration field dissipated, all the electrodes in the MEA except for the electrodes that were initiated were potentiodynamically scanned to determine the potential at which the current threshold was exceeded. Figure 12 shows the results of replicate experiments. The results show that the HNO₃ pretreated MEAs had a deviation of less than 20 mV from the non-interactive control values indicating that persistent interactions have been eliminated. Hence, a treatment known to remove MnS inclusions eliminated persistent interactions.

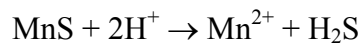
DISCUSSION

Spatial regions of suppression or enhancement in pitting susceptibility varied across the electrode surface as seen in Figure 1. Experimental design enabled separation of interaction factors. The question remains whether the interactions investigated could explain suppressed regions immediately adjacent to the active pit and enhanced pitting occurring around suppressed regions.

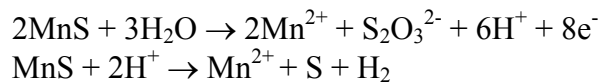
During the growth of large pits, according to the acid pitting mechanism, metal ion hydrolysis takes place within the pit, Cl⁻ and H⁺ ions accumulate within and around the pit, and currents flow from the pit [1]. As currents flow through solution, a potential gradient is formed due to solution resistance indicated by Ohm's law. The ohmic potential gradient that is formed has been shown to cause suppressed pitting in regions adjacent to active primary pits both visually, in Figure 1, and experimentally on MEAs (Figure 5). Experimental results indicate that an increase in the remotely measured potential at which the current threshold was exceeded was seen across an entire electrode surface. Figure 5 shows that an increase as high as 250 mV was seen at a cumulative probability of 50%. Calculations of ohmic potential indicate that rapid drop in ohmic potential occurs and that ohmic potentials are still present at large distances from the pit mouth [10]. These results support the experimental findings. Ohmic potential suppression was found to dominate over other interactive mechanisms and thus results didn't show effects due to concentration gradients and surface damage even though they would be present at the same time due to the acid pitting mechanism.

It is well known that the local solution enhancement occurs due to the acid pitting mechanism, but it has been difficult to measure experimentally due to the small affected region and short time scale [11]. The use of MEAs enables the measurement of these local regions both spatially and temporally. Experiments were conducted where two centrally located rows of the MEA were initiated to form large active pits that would generate concentration gradients of Cl⁻ and H⁺ ions. Active rows were deactivated in order to eliminate ohmic potential effects so only aggressive species enhancement and surface damage would be the only acting effects. The results, in Figure 6 and 7, show that a decrease in E_{pit} was seen on rows 1 through 3 adjacent to active pits. Results indicate that a region three to four pit diameters away from the active pit is affected by aggressive species enhancement or surface damage (Figure 7). The region adjacent to active pits would have the highest concentrations of Cl⁻ and H⁺ ions. These results can be predicted using the results of non-interactive experiments conducted at various Cl⁻ ion concentrations and pHs (Figure 4).

One of the most striking findings is the long persistency of interactions even after five hours (Figure 10). It has been hypothesized that the origin of persistent interactions, in 316 SS, is surface damage caused by aggressive species in solution [4]. The mechanisms of surface could possible be: dissolution of inclusions due to low pH [7], Cr:Fe oxide film alteration [9, 12], oxide film thickening or thinning, or surface/oxide contamination from sulfur or other species [8, 13-15]. It has been well reported that localized corrosion initiates in stainless steels at inclusions, in particular MnS inclusions [8, 11, 14-34]. Many mechanisms of pit initiation at MnS inclusions have been proposed but the basic mechanism is that either the inclusion begins to dissolve or the matrix around the inclusion dissolves leading to the acid pitting mechanism. The low pH causes preferential dissolution of MnS inclusions releasing sulfur species that are known to cause damage to oxide films by suppressing repassivation as well as by initiating further MnS inclusion dissolution [8, 13-15]. It has been hypothesized that MnS inclusions dissolve by chemical dissolution at low potentials [18].



MnS inclusions are argued to decompose electrochemically at high potentials [35]:



Complete or partial dissolution of MnS inclusions can also create crevice environments that are more susceptible [9, 11, 14]. It has been shown that deep narrow inclusions are more dangerous to pitting susceptibility than shallow wide inclusions. Webb showed that stainless steel samples that were tested on the short transverse plane, where MnS inclusions have a small surface area but are deep due to rolling, initiated into stable pitting. Samples that were oriented on either of the other faces, where wide shallow inclusions were found, rarely formed stable pits [11]. The AISI 316 SS wire used to construct MEAs for this study was drawn and contained small surface area inclusion cross-sections on the polished surface. However, these inclusions were deep along the drawing direction. This indicates that the inclusions would be deep unless the end of an inclusion was close to the surface such that the inclusion would be shallow. These deep inclusions would be more dangerous because they would tend to form narrow occluded regions during dissolution. Webb found that deep inclusions tended to only partially dissolve leaving a piece of inclusion at the bottom of the occluded region [11]. Webb attributed partial dissolution of MnS inclusions to oxidation and repassivation of the MnS inclusion, but it is possible that partial dissolution could also have been caused by mixed oxides or presence of less susceptible mixed metal sulfides that did not dissolve away during the tests. The degree of dissolution also depends on time, pH, oxidizing environment, temperature, and chemical composition of the inclusion. AISI 321 stainless steel contains small amounts of Ti that form TiS instead of MnS. The susceptibility of TiS inclusions to dissolution during acid exposure is lower than that of MnS. Therefore, TiS inclusions remain stable while MnS inclusions dissolve resulting in partial dissolution of the inclusion and narrow susceptible crevices [9]. Baroux showed that stainless steels containing MnS inclusions showed a pH dependent pitting potential at fixed Cl⁻ concentrations due to MnS inclusion dissolution while stainless steels that contain TiS inclusions did not show this dependence [7]. It has also been shown that the chromium content of certain regions of inclusions varies. Such variation can produce

inclusions with increased susceptibility compared to other inclusions with a higher Cr content that are more resistance to attack [9, 16].

Exposure conditions that initially passive electrodes adjacent to the active row would experience were simulated by pretreating entire MEAs with HCl solution. Measurements have shown that regions around pits have been found with pHs as low as 0 and chloride concentrations high enough such that salt films form [1, 36-38]. MEAs were pretreated with 1M HCl in order to roughly simulate exposure to these environments when adjacent to a primary pit. Results indicate that severe surface damage occurred during the pretreatment as evidenced by a decrease in E_{pit} in 0.05M NaCl, shown in Figure 11. The surface damage and decrease in E_{pit} caused by HCl pretreatment clearly indicates that solution enhancement adjacent to deactivated pits can have an interactive effect.

In order to determine whether the origin of persistent interactions was associated with damage to MnS and other inclusions, the inclusions were removed by another pretreatment consisting of pickling in 20% HNO₃. Pickling in nitric acid has been used for many years to remove mixed metal oxides and sulfur inclusions from the surface of stainless steels in order to increase pitting resistance [9, 24]. Noh et al. pretreated samples in a series of nitric acid concentrations to show that the exact concentration of nitric acid had a significant impact on MnS dissolution [9]. Their results showed an increasing benefit that translated into the increasing resistance to pit stabilization with increasing HNO₃ concentration with a maximum benefit with 20% HNO₃ at 90°C. This trend was attributed to the dissolution of susceptible inclusions resulting in decreased susceptibility. Above 20% HNO₃ concentration, susceptibility increased. The increases above 20% were caused by the partial dissolution of highly susceptible inclusions resulting in narrow crevices and increased susceptibility. Nitric acid has also been shown to change Cr:Fe ratios in the oxide surface. Moreover, Cr:Fe ratio was shown to increase continuously with increases in nitric acid pretreatment concentration. However, Cr:Fe ratios continue to increase with increasing HNO₃ concentrations even though E_{pit} decreases above 20%. The increase in Cr:Fe ratios despite a corresponding decrease in pitting potential strongly suggests that Cr:Fe ratios have secondary effects on the pitting potential [9, 12, 39].

It was hypothesized that persistent surface damage was caused by damage originating from the aggressive solution gradient that formed around the primary pit during acid pitting [1]. It was hypothesized that the damage to the adjacent surface originates from damage to MnS inclusions. In order to investigate whether MnS inclusions were the source of the persistent surface damage, inclusions were removed prior to testing. MEA samples were pretreated in HNO₃ to remove many inclusions from the surface. Recall that persistent interactions were still seen after five hours on untreated electrodes (Figure 10). As seen in Figure 12, MEAs that were pretreated with HNO₃ prior to persistent interactive testing showed no persistent interactive effects. It is believed that the aggressive solution containing high Cl⁻ and H⁺ ions catalyze MnS dissolution leaving micro-crevices that are highly susceptible even after the aggressive solution has dissipated. These results were confirmed by pretreatment of samples with HNO₃ for one hour followed by pretreatment with 1M HCl for one hour prior to determining E_{pit} in 0.05M NaCl. Results indicate (Figure 11) that electrodes pretreated with HNO₃ were no longer susceptible to inclusion damage caused by reducing HCl. It is hypothesized that the removal of inclusions by HNO₃ treatment leaves a passive electrode surface with very few preferential pitting sites and few environmentally susceptible inclusions that could be damaged. The removal of inclusions prior to persistent

experiments eliminates persistent interactions caused by permanent surface damage. This implicates MnS inclusion damage as the origin of persistent interactions.

CONCLUSIONS

1. Cumulative probability distributions associated with pit stabilization of AISI 316 stainless steel are not normally distributed suggesting that different populations of critical defects or different processes associated with the acid pit stabilization mechanism contribute to pit stabilization on AISI 316 stainless steel. The susceptible tail of the cumulative probability distribution is believed to be associated with a population of large, susceptible MnS inclusions.
2. The AISI 316 stainless steel investigated exhibits increased pit stabilization susceptibility at low pH in HCl solutions, which is consistent with previous studies on stainless steels rich in (MnCr)S inclusions rich in Mn that are prone to dissolution in reducing acids [7].
3. Ohmic potential shielding associated with primary pits consistently suppresses pit stabilization on adjacent electrodes due to the introduction of a large ohmic voltages [2, 4]. The ohmic voltage introduced by primary pits affects the entire population of pit stabilization events similarly regardless of cumulative probability ranking.
4. Accumulation of aggressive ions associated with primary pits consistently promotes pit stabilization and increases pit susceptibility on adjacent electrodes [2, 4]. However, this effect can be dominated by the large ohmic voltage effect when active primary pits emit current. The aggressive ions introduced by primary pits affect the entire population of pit stabilization events similarly regardless of cumulative probability ranking.
5. Accumulation of aggressive ions associated with primary pits promotes surface damage on adjacent electrodes. Surface damage persistently increases pitting susceptibility long after concentrations fields have dissipated. Surface damage particularly alters pit stabilization on the population of pit sites associated with the most susceptible tail in the cumulative probability distribution of pitting potentials.
6. HNO₃ pretreatment eliminates surface damage from nearby pitting that was previously observed to persistently increases pitting susceptibility long after concentrations fields have dissipated. Removal and/or alteration of the population of large, susceptible MnS inclusions associated with the most susceptible tail of cumulative probability distributions is implicated.

ACKNOWLEDGMENTS

The United States Department of Energy, Office of Basic Energy Sciences, Division of Materials Sciences and Engineering supported this project under contract DEFG02-00ER45825 with Dr. Yok Chen as contact monitor. Equipment and software supported by Princeton Applied Research and Scribner Associates, Inc. is gratefully acknowledged. J. L. Hudson is gratefully acknowledged for his contributions to the project.

REFERENCES

1. J. R. Galvele, *J. Electrochem. Soc.*, **123**:464 (1976).
2. T. T. Lunt, V. Brusamarello, J. R. Scully, and J. L. Hudson, *Electrochem. Solid-State Lett.*, **3**:271 (2000).
3. T. T. Lunt, S. T. Pride, J. R. Scully, J. L. Hudson, and A. S. Mikhailov, *J. Electrochem. Soc.*, **144**:1620 (1997).
4. T. T. Lunt, J. R. Scully, V. Brusamarello, A. S. Mikhailov, and J. L. Hudson, *J. Electrochem. Soc.*, **149**:B163 (2002).
5. B. Wu, J. R. Scully, and J. L. Hudson, *J. Electrochem. Soc.*, **144**:1614 (1997).
6. M. Henthorne, *Corros. Sci.*, **26**:511 (1970).
7. B. Baroux, in *Corrosion Mechanisms in Theory and Practice* (P. Marcus and J. Oudar, eds.), Marcel Dekker, Inc., New York, 1995, p. 265.
8. J. Stewart and E. Williams, *Corros. Sci.*, **33**:457 (1990).
9. J. S. Noh, N. J. Laycock, W. Gao, and D. B. Wells, *Corros. Sci.*, **42**:2069 (2000).
10. J. Newman, *J. Electrochem. Soc.*, **113**:1235 (1966).
11. E. G. Webb and R. C. Alkire, *J. Electrochem. Soc.*, **149**:B272 (2002).
12. M. A. Barbosa, *Corros. Sci.*, **23**:1293 (1983).
13. P. Marcus and H. Talah, *Corros. Sci.*, **29**:455 (1989).
14. G. Eklund, *Scand. J. Metall.*, **1**:331 (1972).
15. M. B. Ives and S. C. Srivastava, in *Advances in Localized Corrosion*, Proceedings of the Second International Conference on Localized Corrosion (H. S. Isaacs, U. Bertocci, J. Kruger, and S. Smialowska, eds.), NACE, Orlando, Florida, 1987, p. 295.
16. M. A. Baker and J. E. Castle, *Corros. Sci.*, **34**:667 (1993).
17. A. P. Bond and E. A. Lizlovs, *J. Electrochem. Soc.*, **November 1968**:1130 (1968).
18. C. S. Brossia, in *Critical Factors in Localized Corrosion III* (R. G. Kelly, G. S. Frankel, P. M. Natishan, and R. C. Newman, eds.), ECS, 1998, p. 327.
19. N. J. E. Dowling, C. Duret-Thual, G. Auclair, J. P. Audouard, and P. Combrade, *Corrosion*, **51**:343 (1995).
20. G. Eklund, *J. Electrochem. Soc.*, **121**:467 (1974).
21. J. N. Harb and R. C. Alkire, *J. Electrochem. Soc.*, **138**:2594 (1991).
22. R. Ke and R. Alkire, *J. Electrochem. Soc.*, **Vol 139, No. 6**:1573 (1992).
23. R. Ke and R. Alkire, *J. Electrochem. Soc.*, **142**:4056 (1995).
24. R. M. Kain, in *Corroison 91 The NACE Conference and Corrosion Show*, Paper Number 508, NACE, Cincinnati Ohio, 1991.
25. C. H. Paik and R. C. Alkire, *J. Electrochem. Soc.*, **148**:B276 (2001).
26. A. M. Riley, D. B. Wells, and D. E. Williams, *Corros. Sci.*, **32**:1307 (1991).
27. A. J. Sedriks, *Int. Met. Rev.*, **28**:295 (1983).
28. M. Smialowski, Z. Szklarska-Smialowska, M. Rychcik, and A. Szummer, *Corros. Sci.*, **9**:123 (1969).
29. T. Suter and H. Bohni, *Electrochim. Acta*, **42**:3275 (1997).
30. Z. Szklarska-Smialowska, *Corrosion*, **28**:388 (1972).
31. E. G. Webb and R. C. Alkire, *J. Electrochem. Soc.*, **149**:B280 (2002).
32. E. G. Webb and R. C. Alkire, *J. Electrochem. Soc.*, **149**:B286 (2002).
33. E. G. Webb, C. H. Paik, and R. C. Alkire, *Electrochem. Solid-State Lett.*, **4**:B15 (2001).
34. G. Wranglen, *Corros. Sci.*, **14**:331 (1974).

35. S. E. Lott and R. C. Alkire, *J. Electrochem. Soc.*, 136:973 (1989).
 36. T. Suzuki, M. Yamabe, and Y. Kitamura, *Corrosion*, 29 No. 1:18 (1973).
 37. B. E. Wilde and E. Williams, *Electrochim. Acta*, 16:1971 (1971).
 38. G. Butler, C. K. Ison, and A. D. Mercer, *Br. Corros. J.*, 6:31 (1971).
 39. G. Hultquist and C. Leygraf, *Corrosion*, 36:126 (1980).

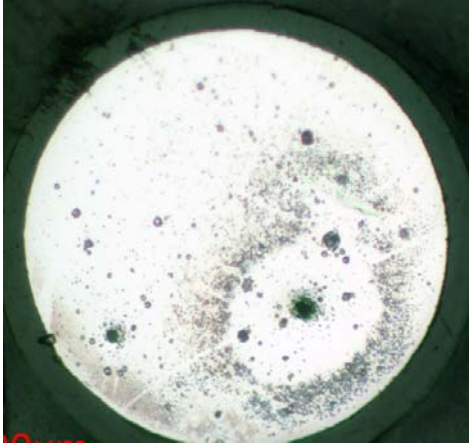


Figure 1. Visual observations of regions of enhanced and suppressed localized corrosion around large primary pits on AISI 316 stainless steel potentiodynamically scanned in 0.05 M NaCl (pH 6.8) at 47°C.

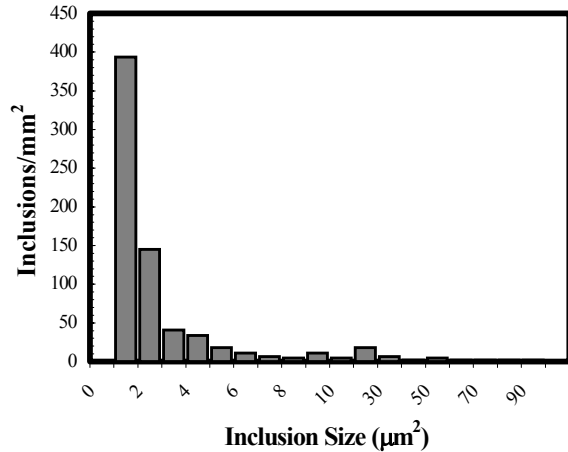


Figure 2. Distribution of inclusions in AISI 316 SS wire cross section.

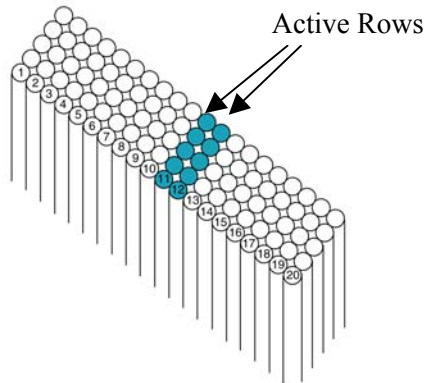


Figure 3. Arrangement of multi-electrode arrays in a 5x20 close packed configuration consisting of 250 µm AISI 316 SS wires, mounted in epoxy, and polished to a planar face.

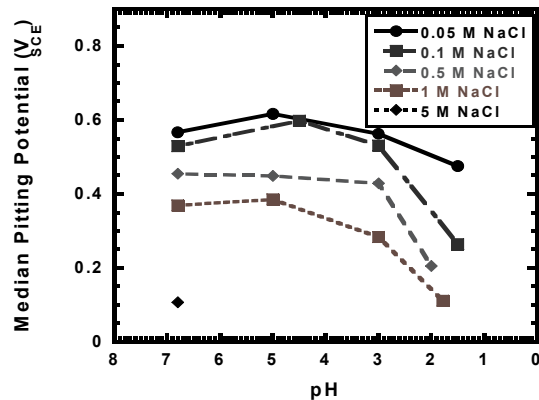


Figure 4. Median E_{pit} for AISI 316 SS in various NaCl + HCl solutions at the indicated pH levels at 47°C. The data was generated from non-interactive control experiments on 250 µm diameter wires.

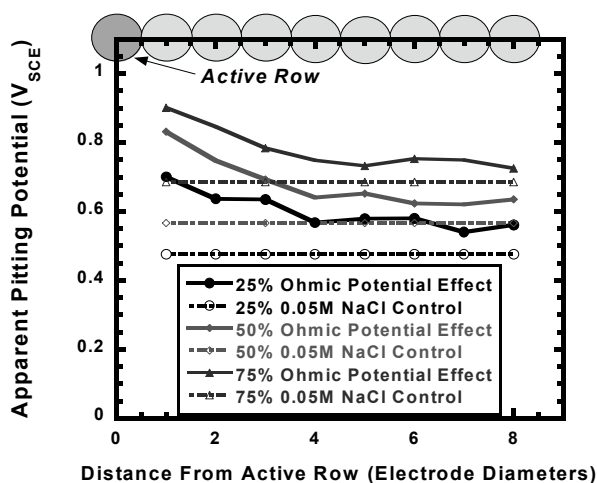


Figure 5. Remotely sensed applied potentials at which the pit current threshold was exceeded for AISI 316 SS, in 0.05 M NaCl (pH 6.8) at 47°C. The applied potentials required for pit stabilization are elevated due to ohmic potential shielding.

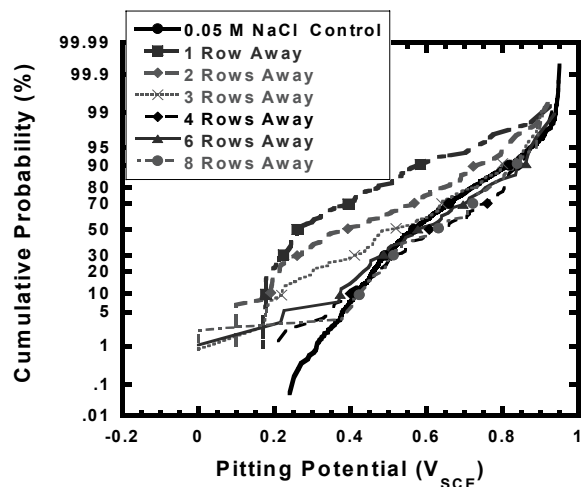


Figure 6. The cumulative probability of pit stabilization at a given potential for AISI 316 SS in 0.05 M NaCl (pH 6.8) at 47°. Results are shown as a function of MEA row when a local aggressive solution was developed by active pitting on two MEA electrode rows.

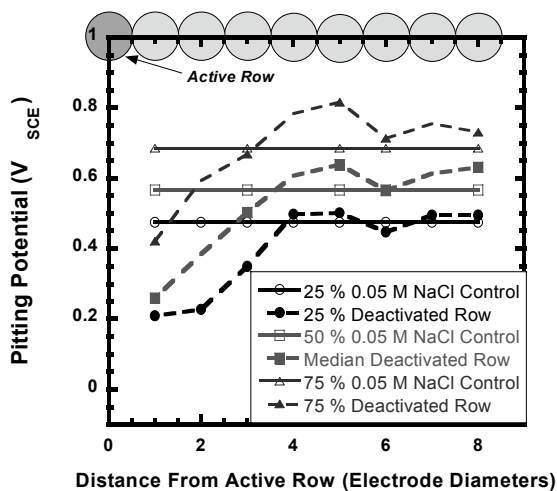


Figure 7. The IR-free pitting potential associated with cumulative probabilities of 25%, 50%, and 75% for AISI 316 SS, in 0.05 M NaCl (pH 6.8) at 47°C as a function of distance from the active row of electrodes. E_{pit} was determined in scans immediately after primary pit rows were deactivated.

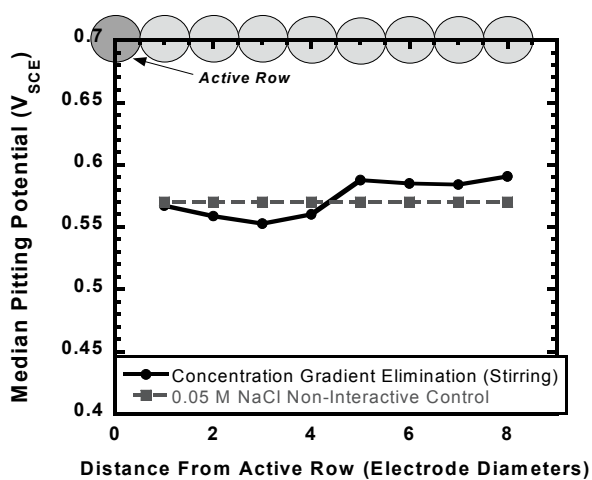


Figure 8. The IR-free median pitting potential of AISI 316 SS in 0.05 M NaCl (pH 6.8) at 47°C, as a function of MEA row. Solutions were stirred during primary pit growth to eliminate concentration gradients during propagation. The remaining passive electrodes were immediately scanned after primary pit deactivation.

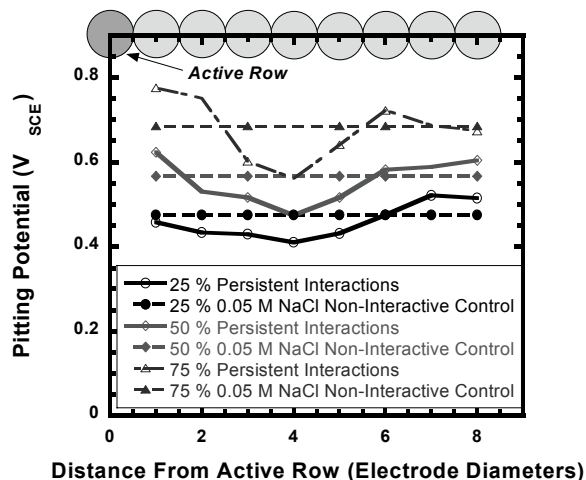


Figure 9 The IR-free pitting potential at cumulative probabilities of 25%, 50%, and 75% for AISI 316 SS in 0.05 M NaCl (pH 6.8) at 47°C, as a function of distance from the active row of electrodes. E_{pit} was determined after a 15-minute rest period to allow aggressive solution concentrations to dissipate.

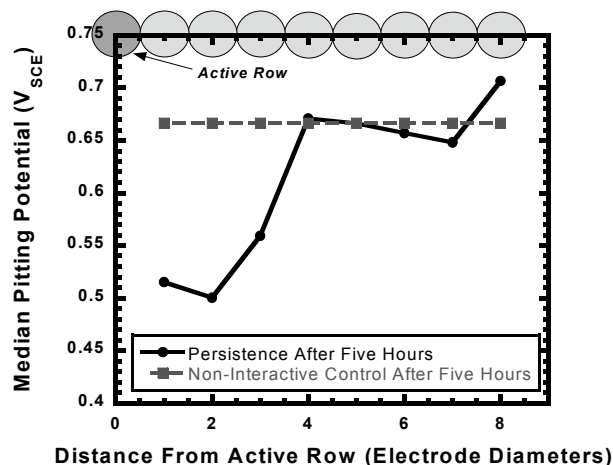


Figure 10. Median IR-free E_{pit} , as a function of MEA row, for AISI 316 SS in 0.05 M NaCl (pH 6.8) at 47°C, as affected by 5-hour exposure to aggressive species from primary pits.

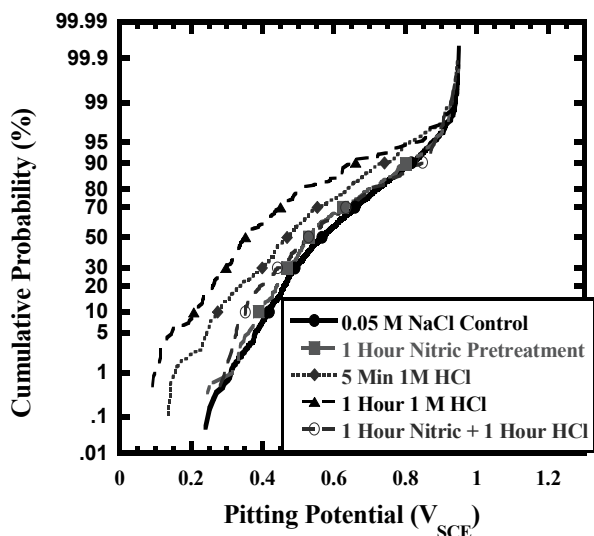


Figure 11. Cumulative probability of pit stabilization for AISI 316 SS in 0.05 M NaCl (pH 6.8) at 47°C after HCl and HNO₃ pretreatment of electrodes.

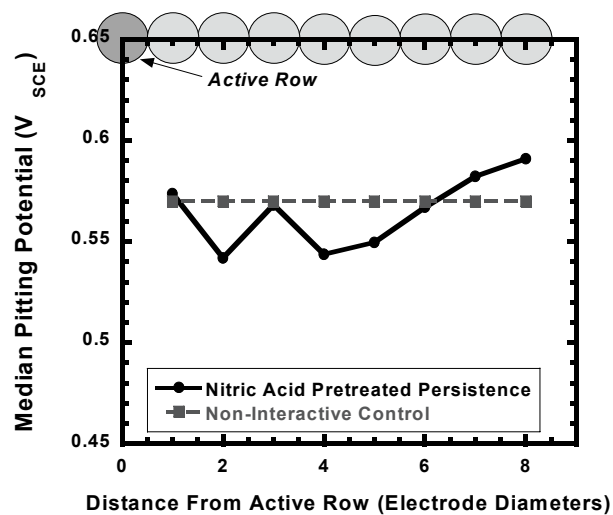


Figure 12. Median-IR free E_{pit} , as a function of MEA row, for AISI 316 SS in 0.05 M NaCl (pH 6.8) at 47°C pretreated with nitric acid prior to aggressive species induced surface damage from primary pits.